Journal of Alloys and Compounds 908 (2022) 164621

Contents lists available at ScienceDirect

Journal of Alloys and Compounds

journal homepage: www.elsevier.com/locate/jalcom

Research Article

Green-emitting Bi^{3+}-doped $La_2SrSc_2O_7$ phosphor for pc-WLED lighting: Luminescent properties and energy transfer strategy

Wei Yan[a,b], Yi Wei[b], Maxim S. Molokeev[c,d,e], Song Wang[a,*], Guogang Li[b,*]

[a] Hubei Key Laboratory of Low Dimensional Optoelectronic Materials and Devices, Hubei University of Arts and Science, Xiangyang, 441053 Hubei, PR China
[b] Engineering Research Center of Nano-Geomaterials of Ministry of Education, Faculty of Materials Science and Chemistry, China University of Geosciences, 388 Lumo Road, Wuhan 430074, PR China
[c] Laboratory of Crystal Physics, Kirensky Institute of Physics, FRC KSC SB RAS, Krasnoyarsk 660036, Russia
[d] Research and Development Department, Kemerovo State University, Kemerovo 650000, Russia
[e] Siberian Federal University, Krasnoyarsk 660041, Russia

ARTICLE INFO

Article history:
Received 19 October 2020
Received in revised form 7 March 2022
Accepted 15 March 2022
Available online 17 March 2022

Keywords:
Green phosphor
Bi^{3+}
Energy transfer strategy
Color tuning
Pc-WLED devices

ABSTRACT

The crystal structure, photoluminescence properties, thermal stability and corresponding mechanisms of the novel Bi^{3+}, Eu^{3+}-doped $La_2SrSc_2O_7$ (LSS) phosphors have been measured and analyzed in details. The emission spectrum of LSS: 1.0%Bi^{3+} phosphor shows a novel green emission centered at 530 nm under 340 nm excitation, which is attributed to the $^3P_1 \rightarrow {}^1S_0$ transition of Bi^{3+} ions. By designing $Bi^{3+} \rightarrow Eu^{3+}$energy transfer strategy, luminescence colors of LSS: 1.0%Bi^{3+}, yEu^{3+} (y = 0–5.0%) phosphors can be tuned from green to orange with increasing Eu^{3+} concentration, which achieve multiple emission colors in LSS host. The photoluminescence decay curves, average decay lifetimes, energy transfer efficiency and time-resolved emission spectra of LSS: 1.0%Bi^{3+}, yEu^{3+} (y = 0–5.0%) phosphors prove the existence of energy transfer from Bi^{3+} to Eu^{3+}. The prototype pc-WLED device with green-emitting LSS: 1.0%Bi^{3+} possesses high color rendering index (CRI = 96.0) and low correlated color temperature (CCT = 4306 K). These results provide clear evidences that LSS: $Bi^{3+}$and LSS: 1.0%Bi^{3+}, Eu^{3+} phosphors would be novel promising green-to-orange tunable phosphor candidates for pc-WLED applications.

1. Introduction

Phosphor-converted white-light-emitting diodes (pc-WLED) has become the popular lighting implements for their advantages, such as high efficiency, energy conservation, environmental friendliness, long operation lifetimes, and so on [1–5]. There are two methods to fabricate pc-WLED devices. Firstly, pc-WLED devices can be fabricated by commercial yellow $Y_3Al_5O_{12}$: Ce^{3+} (YAG: Ce^{3+}) phosphor and blue LED chip [6–8]. However, due to the lack of red component, they emit cold white light with high correlated color temperature (CCT > 4500 K) and low color rendering index (CRI < 75), which would make eyes uncomfortable [9–11]. In order to overcome these drawbacks, pc-WLED devices can also be fabricated by alternative method that combines red, green, and blue phosphors with near-ultraviolet (n-UV) LED chips (350–410 nm) [12–15]. Thus, warm white light is achieved due to the supplement of red component. However, these drawbacks such as spectral reabsorption, improper excitation location and unsuitable spectral profiles still exist [16]. In other words, the lighting quality of pc-WLED devices is determined by the luminescence properties of fabricated phosphors. Besides, people's eyes are more sensitive to green light than blue or red light [17]. Therefore, photoluminescence quantum yield of green component is also a critical index for lighting quality of pc-WLED devices. Moreover, green phosphors can supply spectra range from 492 to 577 nm for covering the whole visible light region, which also improves lighting quality of pc-WLED devices. Consequently, it is necessary to explore highly-efficient green phosphors excited by n-UV/UV LED chips to improve the lighting quality of pc-WLED devices.

As a representative non-rare-earth metal ion, Bi^{3+}-doped phosphors have attracted much attention in recent years due to the abundant emission colors covering whole visible and even UV or n-UV regions. The sensitivity of Bi^{3+} to environment is attributed to the naked 6s electrons. The transition of $^3P_1$-$^1S_0$ and $^1P_1$-$^1S_0$ exerts the possibility for the multi-emission colors for Bi^{3+}. In other words, bond length, coordination number, lattice symmetry and other factors can influence the luminescent properties of Bi^{3+}-doped phosphors [18–21]. For example, La_3BWO_9:Bi^{3+} phosphor shows a novel

* Corresponding authors.
E-mail addresses: wangsong1984@126.com (S. Wang), ggli@cug.edu.cn (G. Li).

https://doi.org/10.1016/j.jallcom.2022.164621
0925-8388/

yellow emission [22]. $ABZn_2Ga_2O_7$:Bi^{3+} (ABZGO, A = Ca, Sr; B = Ba, Sr) phosphors realized tunable yellow-orange optical properties by cation substitution [23]. Bi^{3+}-doped $Ba_3Sc_4O_9$ phosphors can achieve color tuning from a green or a bluish green emission to yellow under different excitation [24]. Besides, it is well known that Eu^{3+}-doped phosphors usually show red emission with the maximum peak around 613 nm due to the intra-configurational 4–4f transitions. However, the improper excitation position of Eu^{3+}-doped phosphors limits practical application [25–28]. There are several ways for phosphors to realize luminescence modification such as “doping level control”, “local lattice modification strategy”, and “energy transfer strategy” [29,30]. Energy transfer strategy is the most common method to realize luminescence modification. For energy transfer strategy from Bi^{3+} to Eu^{3+}, Bi^{3+} ion can act as effective sensitizer for Eu^{3+} to achieve energy transfer in different phosphors [31–33]. If Bi^{3+} co-dopes into the Eu^{3+}-activated phosphors as a sensitizer, the red emission can be realized and effectively excited by blue or n-UV/UV chips. For example, energy transfer from Bi^{3+} to Eu^{3+} realized the systematic luminescence tuning from bluish-green to red in $(Sr,Ba)_2LaGaO_5$ [34]. Equally, under UV excitation, warm white light can be achieved by adjusting content ratio of Bi^{3+} and Eu^{3+} in $Sr_3YAl_2O_{7.5}$ host [35]. Also, the luminescence colors of $SrLu_2O_4$: Bi^{3+}, yEu^{3+} (y = 0–12.5%) were tuned from blue to red by designing energy transfer strategy [36]. Therefore, energy transfer strategy is a reliable method to achieve color-tuning in Bi^{3+} and Eu^{3+}co-doped phosphors for practical applications.

In this work, a series of novel $La_2SrSc_2O_7$ (LSS): xBi^{3+} (x = 0.3–3.0%) and LSS: 1.0%Bi^{3+}, yEu^{3+} (y = 0.5–5.0%) phosphors were synthetized by traditional high-temperature solid-state method. The powder X-ray diffraction (XRD) patterns and Rietveld refinement results testify the phase purity of as-prepared phosphors. The novel LSS structure is mainly composed of [$La1/Sr1O_{12}$], [$La2/Sr2O_9$] and [ScO_6] polyhedra. Under 340 nm excitation, novel LSS: 1.0%Bi^{3+} phosphor shows a green emission peaking at 530 nm in the range of 400–725 nm. According to the radius matching rules and the Gaussian fitting analysis, Bi^{3+} tends to occupy two types of La^{3+} sites in LSS host. The temperature-dependent luminescence properties and relative mechanism of LSS: Bi^{3+} phosphors were systematically investigated. The dipole–dipole interaction took the main responsibility for concentration quenching phenomenon of LSS: xBi^{3+} (x = 0.3%–3.0%) phosphors. Moreover, the energy transfer strategy from Bi^{3+} to Eu^{3+} was designed in LSS phosphors. The emission color can be tuned from green to orange with the increase of Eu^{3+} concentration. The pc-WLED device fabricated by LSS: 1.0%Bi^{3+}, commercial red $CaAlSiN_3$: Eu^{2+} phosphor and 370 nm LED chip shows relatively high CRI (96.0) and low CCT (4306 K) values. Therefore, these LSS phosphors have potential application in practical pc-WLED devices.

2. Experimental section

2.1. Materials and preparation

$La_2SrSc_2O_7$ (LSS) host, LSS: xBi^{3+} (x = 0.3%, 0.5%, 0.7%, 1.0%, 2.0%, 3.0%) phosphors, and LSS:1.0%Bi^{3+}, yEu^{3+} (y = 0.5%, 1.0%, 2.0%, 3.0%, 5.0%) phosphors were prepared via a traditional high-temperature solid-state reaction. Stoichiometric amounts of raw materials La_2O_3 (99.99%, Aladdin), $SrCO_3$ (99.9%, Aladdin), Sc_2O_3 (99.99%, Aladdin), Bi_2O_3 (99.99%, Alfa Aesar), and Eu_2O_3 (99.99%, Sigma-Aldrich) were weighed, mixed together and ground sufficiently for 30 mins in an agate mortar with pestle, then the power mixtures were placed into aluminum oxide crucibles and sintered in a tube furnace at 1500 °C for 8 h in air. After the calcination process, the samples were cooling down to room temperature naturally and crushed for 10 min, achieving the final phosphor powders.

2.2. Measurement and characterization

XRD data of all the samples was identified by a D8 Focus diffractometer with Ni-filtered Cu Kα (2θ = 5–120°, λ = 1.540598 Å). Rietveld refinement and the texture analysis were performed with General Structure Analysis System (GSAS) software based on XRD data. The morphologies, energy-dispersive X-ray spectrum (EDS) and elemental mapping analysis of the samples were inspected by a field emission scanning electron microscope (FE-SEM, S-4800, Hitachi). The Diffuse reflectance spectra (DRS) were measured using UV–visible diffuse reflectance spectroscopy UV-2550 PC (Shimadzu Corporation, Japan). X-ray photoelectron spectroscopy (XPS) measurements were attained from the Mg Kα radiation source (Kratos XSAM-800 spectrometer). The photoluminescence excitation (PLE) and emission (PL) spectra of all samples were measured by using fluorescence spectrometer (Fluoromax-4 P, Horiba Jobin Yvon, New Jersey, USA) equipped with a 150 W xenon lamp as the excitation source, and both the excitation and the emission spectra were set up to be 1.0 nm with the width of the monochromator slits adjusted as 1.0 nm. The photoluminescence decay curves and the time-resolve emission spectra were performed by a Lecroy Wave Runner 6100 Digital Osillosccope (1 GHz) using a tunable laser (pulse width = 4 ns; gate = 50 ns) as the excitation source (Contimuum Sunlite OPO). Photoluminescence quantum yield (PLQY) measurement are collected on absolute PL quantum yield measurement system (Edinburgh Instruments FLS1000) under 340 nm excitation wavelength. Commission Internationale de l′Eclairage chromaticity color coordinates (CIE), CRI, and the CCT of the pc-WLEDs devices were measured by using an integrating sphere with an analyzer system (tarspec SSP6612). All the above measurements were performed at room temperature. What is more, the temperature-dependent (25–250 °C) PL spectra were measured on a fluorescence spectrophotometer (Edinburgh Instruments FLSP-920) with a temperature controller.

2.3. pc-WLED devices fabrication

The pc-WLED devices were fabricated by combining the mixture of the representative LSS: 1.0%Bi^{3+} phosphor, LSS: 1.0%Bi^{3+}, 5.0%Eu^{3+} phosphor and 370 nm InGaN chips. The commercial red $CaAlSiN_3$: Eu^{2+} phosphor, blue $BaMgAl_{10}O_{17}$:Eu^{2+} phosphor and commercial green $(Ba,Sr)_2SiO_4$: Eu^{2+} phosphor were also used as the participants in these above pc-WLED devices. Appropriate amounts of phosphors were added into the epoxy resins and mixed thoroughly about 20 min. The acquired mixture was coated on the surface of the 370 nm InGaN chips and dried at 70 °C to produce pc-WLED devices. All measurements were carried out at 200 mA driving current.

3. Results and discussion

3.1. Phase recognition and the luminescence properties of LSS: Bi^{3+} phosphors

Fig. 1**a** displays the XRD patterns of LSS: xBi^{3+} (x = 0.3–3.0%) phosphors and the standard LSS (PDF-79–2362). It is noteworthy that all the diffraction peaks are well indexed to the standard LSS host, which demonstrates the phase purity of LSS: xBi^{3+} (x = 0.3–3.0%) samples. In order to investigate the crystal structure of LSS: xBi^{3+} (x = 0.3–3.0%) samples, the powder XRD data of representative LSS: 1.0%Bi^{3+} phosphor is detected at room temperature with 2θ range of 5–120° for Rietveld refinement analysis. The experimental (black circle) and calculated (red line) XRD profiles together with their difference (blue line) between LSS: 1.0%Bi^{3+} and LSS host are exhibited in Fig. 1**b**. The refinement is well-convergent due to low *R*-factors (R_{wp} = 6.69% and R_p = 4.65%), which proves that stable and pure sample was obtained. Moreover, the final Rietveld

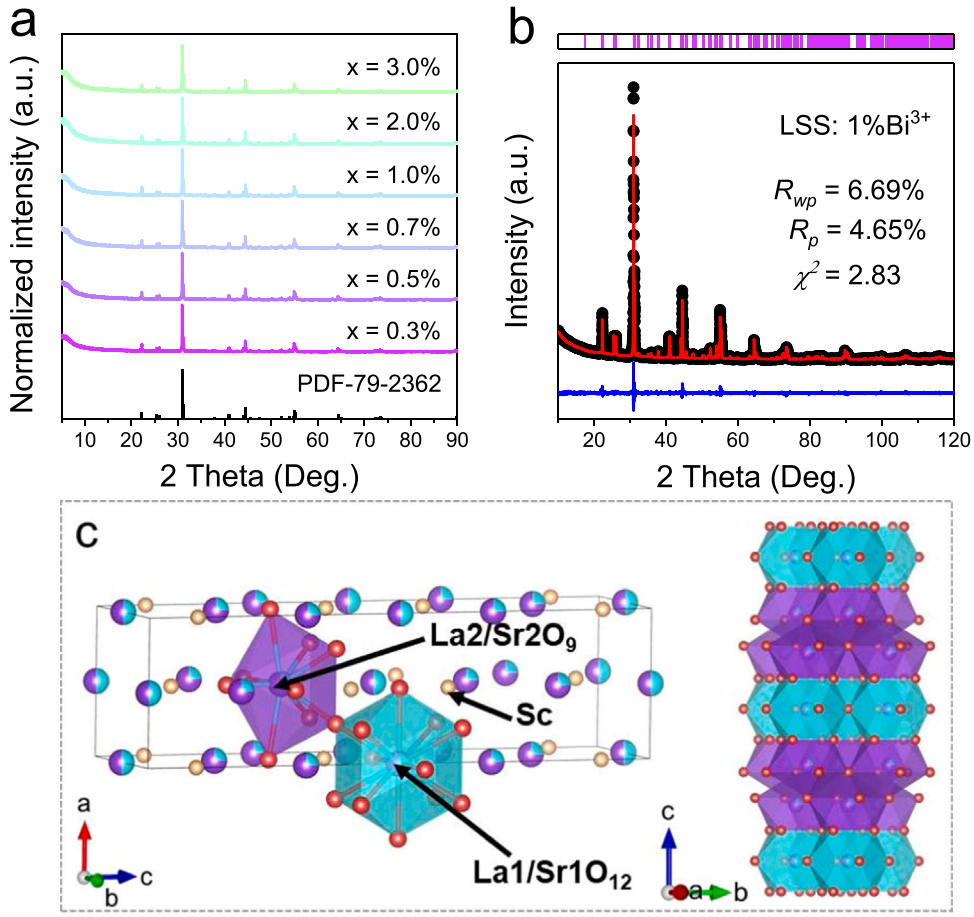

Fig. 1. (a) XRD patterns of LSS: xBi^{3+} (x = 0.3–3.0%) phosphors and the standard LSS (PDF-79–2362). (b) Rietveld refinement XRD data of representative LSS: $1.0\%Bi^{3+}$ phosphor with measured data (black circles), fitted data (red line), difference (blue line) and Bragg position (purple vertical bar). (c) The crystal structure of LSS host in different direction and the polyhedral structure of $La1/Sr1O_{12}$, $La2/Sc2O_9$.

Table 1
The main crystal parameters and Rietveld refinement results of representative LSS: $1.0\%Bi^{3+}$ phosphor.

Parameters	$La_2SrSc_2O_7$: $1.0\%Bi^{3+}$
Space group	*Fmmm*
a, Å	5.7818 (5)
b, Å	5.7367 (5)
c, Å	20.534 (2)
V, Å^3	681.08(11)
Z	4
R_{wp}, %	6.69
R_p, %	4.65
χ^2	2.83

refinement results and main parameters of processing are presented in Table 1. According to Rietveld refinement results, LSS: $1.0\%Bi^{3+}$ sample belongs to *Fmmm* space group with unit cell parameters *a* = 5.7818 (5) Å, *b* = 5.7367 (5) Å, *c* = 20.534 (2) Å and cell volume *V* = 681.08 (11) Å^3. As shown in Fig. 1**c**, there are two types of La sites in LSS host, which are intermixed with Sr in different coordination. The occupations Occ(La) and Occ(Sr) are refined with linear restrictions, which are $Occ_{0.5}(La1) + Occ_{0.5}(Sr1) = 1$ and $Occ_{0.75}(La2) + Occ_{0.25}(Sr2) = 1$, respectively. La1/Sr1 is at *4b* site with "*mmm*" symmetry, forming [$La1/Sr1O_{12}$] polyhedron. While La2/Sr2 are coordinated by nine adjacent O atoms, forming [$La2/Sr2O_9$] at *8i* with "*mm2*" symmetry. Besides, there is only one type of [ScO_6] polyhedron in LSS host, which also locates at *8i* with "*mm2*" symmetry. [$La1/Sr1O_{12}$] and [$La2/Sr2O_9$] polyhedra connect with each other by sharing face, forming the fundamental three-dimensional layered framework. Considering the same charge valence and similar ionic radius, Bi^{3+} ions (*r* = 1.03, CN = 6; *r* = 1.17, CN = 8) prefer to occupy La^{3+} sites (*r* = 1.16, CN = 8) rather than Sr^{2+} sites (*r* = 1.26, CN = 8) or Sc^{3+} (*r* = 0.745, CN = 6) [37,38].

In order to explore the morphologies of these as-prepared samples and prove that Bi^{3+} activator ions are successfully doped into LSS host, SEM image, corresponding elemental mapping analysis and the EDS analysis of the representative LSS: $1.0\%Bi^{3+}$ phosphor are performed. As shown in Fig. 2**a**, the as-prepared LSS: $1.0\%Bi^{3+}$ phosphor is assembled by irregular particles of about 6–10 μm in diameter. The corresponding elemental mapping analysis for La, Sr, Sc, O and Bi elements in LSS: $1.0\%Bi^{3+}$ phosphor is shown in Figs. 2**b-2f**, in which all above elements uniformly distribute throughout the whole viewing area with clear boundaries. The EDS data and the corresponding atom percentage of LSS: $1.0\%Bi^{3+}$ sample are shown in Figs. 2**g** and 2**h**, in which the ratio of O:La:Sr:Sc:Bi is 68.73:14.96:9.89:12.07:0.96, which is very close to the theoretical atomic ratio in LSS: $1.0\%Bi^{3+}$ phosphor. These results demonstrate the successful synthesis of LSS: $1.0\%Bi^{3+}$ phosphor and the incorporation of Bi^{3+}.

The optical band gap (E_g) value is the vital factor to judge the efficient luminescence properties of activator in a host, which can be obtained from the diffuse reflectance spectra (DRS). [39,40] The DRS of LSS host is shown in Fig. 3**a**. A strong absorption between 200 and 330 nm can be observed due to the host absorption. Accordingly, E_g values can be calculated by Kubelka-Munk absorption function F(*R*) with the following equations: [41,42].

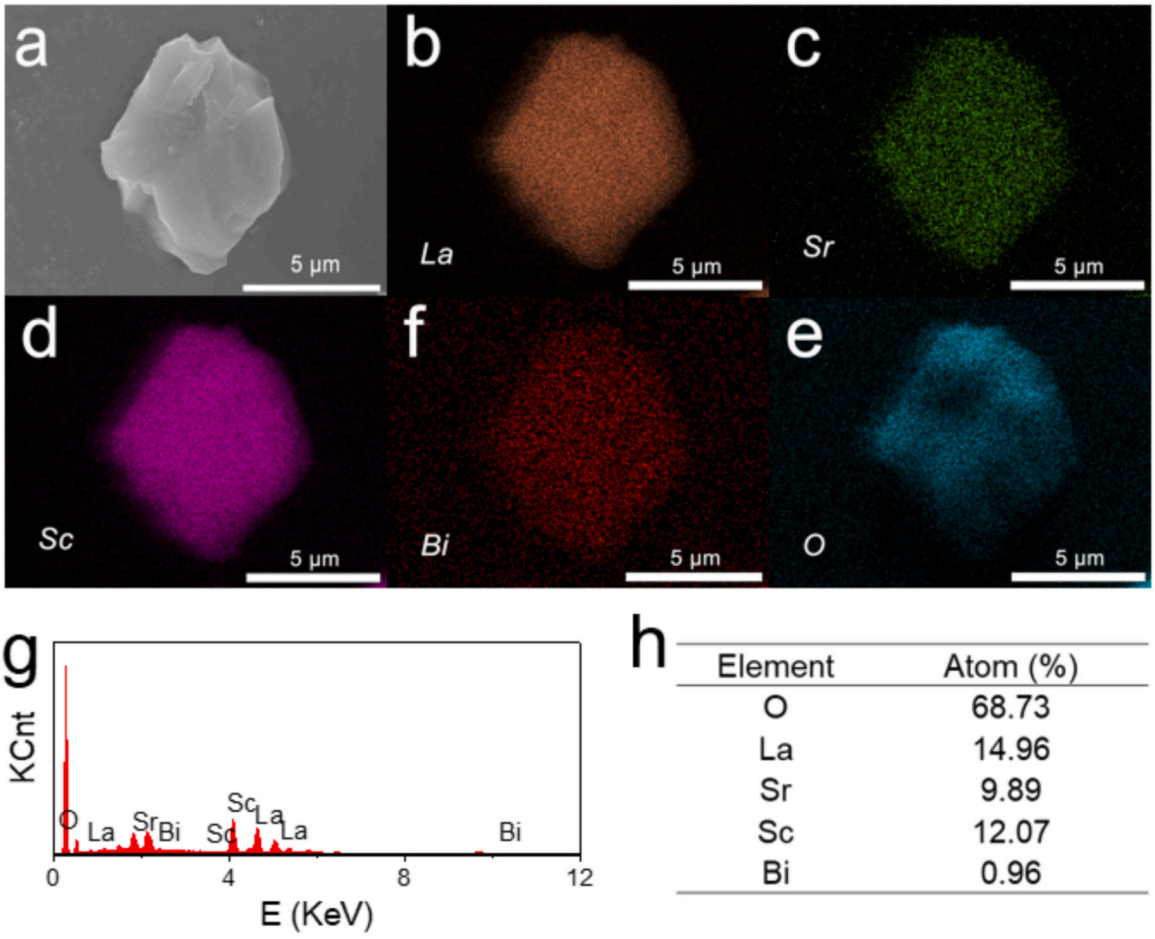

Fig. 2. (a) SEM image, (b-f) corresponding elemental mapping analysis for La, Sr, Sc, O, and Bi elements of representative LSS: 1.0%Bi^{3+} phosphor. (g) The EDS data of the representative LSS: 1.0%Bi^{3+}. (h) The atom percentage in LSS: 1.0%Bi^{3+} phosphor.

$$F(R) = (1 - R)^2/(2R) \quad (1)$$

$$[h\nu F(R)]^n = A(h\nu - E_g) \quad (2)$$

where R represents the measured diffuse reflectance coefficient (%), $h\nu$ is photon energy, $n = 2$ or $1/2$ corresponds to a direct or an indirect band gap, and A stands for the absorption constant. As shown in Fig. 3**b**, the direct band gap value of LSS is 2.08 eV. It indicates that LSS is an appropriate host for rare earth and Bi^{3+} activator ions doping. As shown in Fig. 3**c**, the XPS spectrum of the representative LSS: 1.0%Bi^{3+} phosphor shows the peaks position at 164.05 eV and 158.70 eV, which correspond to the existence of trivalent Bi element. [43] The result further proves the successful incorporation of Bi^{3+} ions into LSS host.

In order to investigate the photoluminescence properties of LSS: xBi^{3+} (x = 0.3%–3.0%) phosphors, PLE spectra of LSS: x%Bi^{3+} (x = 0.3%–3.0%) were measured (Fig. 4**a**), which show broad excitation band ranging from 250 to 425 nm (monitored at 530 nm). It means that the as-prepared samples can be well excited by blue or n-UV LED chips. Under 340 nm excitation (in Fig. 4**b**), novel

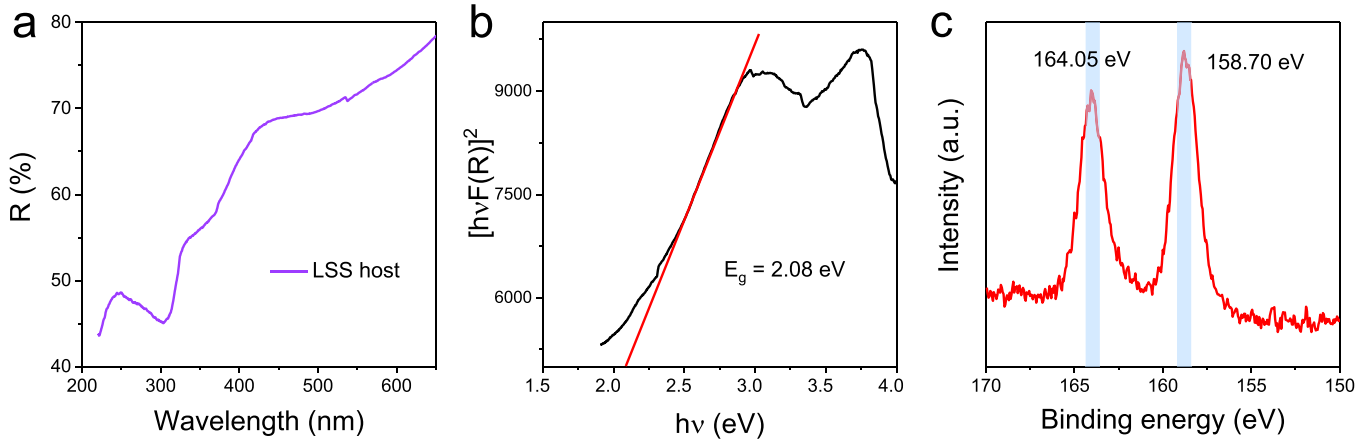

Fig. 3. (a) The Diffuse reflectance spectra of LSS host. (b) Optical band gap calculation for LSS host. (c) XPS spectrum of Bi in LSS: 1.0%Bi^{3+} phosphor.

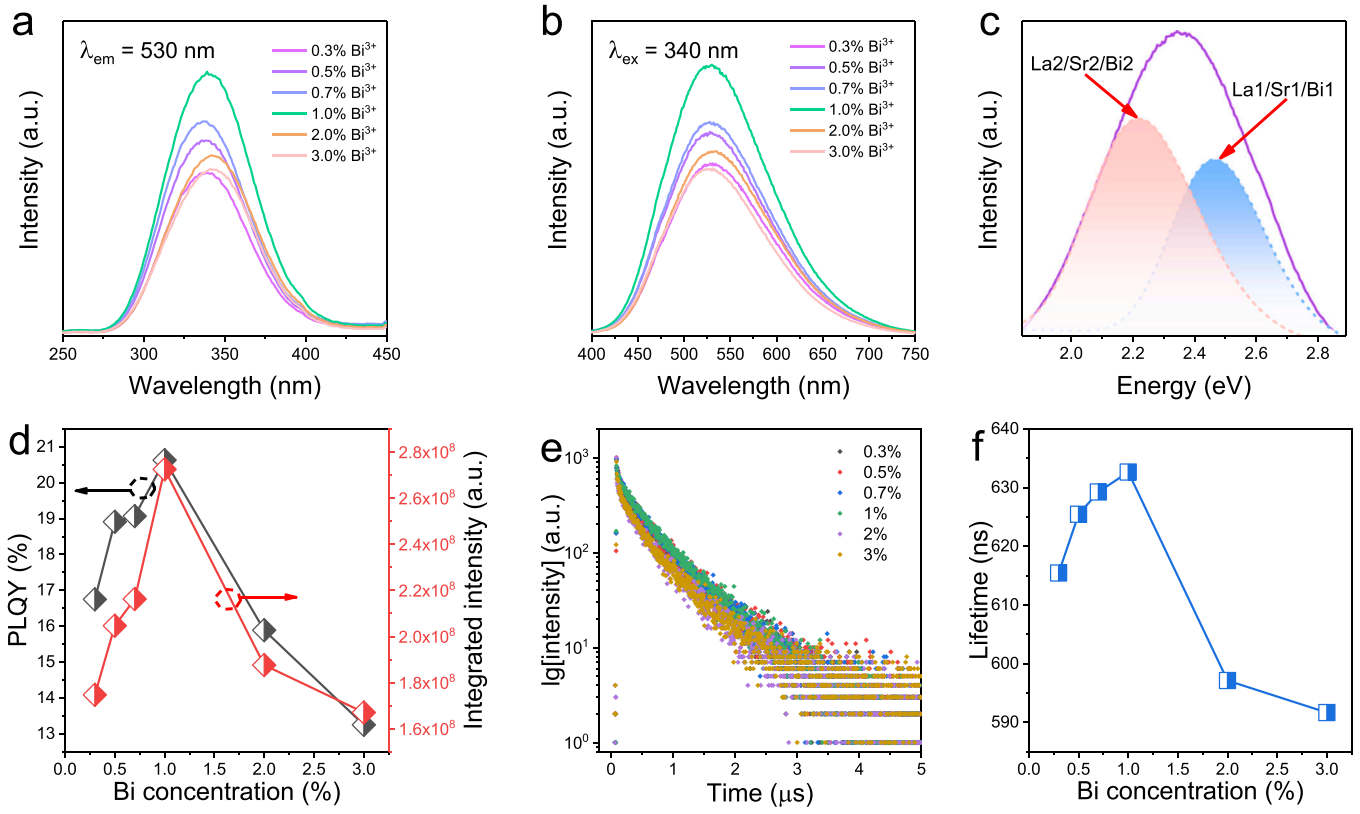

Fig. 4. (a) PLE spectra of LSS: 1.0% Bi^{3+} (monitoring at 530 nm) and (b) PL spectra of LSS: xBi^{3+} (x = 0.3–3.0%) (λ_{ex} = 340 nm). (c) The Gaussian fitting of LSS: 1.0%Bi^{3+} PL spectra. (d) The photoluminescence quantum yield (PLQY) and integrated intensity of LSS: xBi^{3+} (x = 0.3% −3.0%) as a function of Bi^{3+} concentration. (e) The photoluminescence decay curves (λ_{ex} = 375 nm, λ_{em} = 530 nm) of LSS:xBi^{3+} (x = 0.3–3.0%). (f) The lifetime value as function of Bi^{3+} concentration in LSS:xBi^{3+} (x = 0.3–3.0%).

green-emitting LSS: xBi^{3+} (x = 0.3–3.0%) phosphors in the range of 400–725 nm are obtained (centered at 530 nm), which is attributed to $^3P_1 \rightarrow {}^1S_0$ transitions of Bi^{3+} ions. [44,45] As illustrated in Fig. 4**b**, PL spectra of LSS: xBi^{3+} (x = 0.3–3.0%) phosphors are always uniform crossing entire Bi^{3+} concentrations. In order to further discuss the emission behavior of LSS: Bi^{3+} phosphor, the Gaussian fitting analysis of PL spectrum of the representative LSS: 1.0%Bi^{3+} phosphor is shown in Fig. 4**c**. The PL spectrum of the representative LSS: 1.0%Bi^{3+} phosphor can be deconvoluted into two Gaussian bands center at 558 nm (2.46 eV) and 504 nm (2.21 eV), respectively. This result indicates that Bi^{3+} ions would substitute in the two types of La^{3+} sites. On the basis of Van Uitert empirical equation: [46].

$$E(cm^{-1}) = Q\left[1 - \left(\frac{V'}{4}\right)^{1/v} \times 10^{-(nrE)/80}\right] \quad (3)$$

where E is the emission peak position of Bi^{3+} ions, Q represents the energy for the lowest p-band edge of the free Bi^{3+} ions, which is a constant for certain cation, V' stands for the valence of the ion (V'= 3 for Bi^{3+}), n means the number of anions in the immediate shell about the Bi^{3+}, r signifies the radius (Å) of the cation replaced by the Bi^{3+}, and E is the electron affinity of the atoms that form anions (eV). Herein, the value of E increases with n and r becoming larger. Therefore, the fitted emission peak at 504 nm (2.46 eV) is attributed to emission from [La1/Sr1/Bi1O_{12}] polyhedra, and another fitting peak at 558 nm (2.22 eV) is ascribed to emission originated from [La2/Sr2/Bi2O_9] polyhedra (Fig. 4**c**).

Fig. 4**d** shows the photoluminescence quantum yield (PLQY) and integrated PL intensity of LSS: xBi^{3+} (x = 0.3%–3.0%) phosphors as a function of Bi^{3+} concentrations (x). Obviously, PLQY and integrated intensity exhibit similar variation trend. It can be found that the PLQY and PL intensity of LSS: xBi^{3+} (x = 0.3%–3.0%) phosphors show gradually increasing trend with the increase of Bi^{3+} concentrations (x) until it reaches a maximal value at x = 1.0%. Then they decrease with further increasing Bi^{3+} concentration (x) owing to the concentration quenching phenomenon. The increasing Bi^{3+} concentrations (x) will lead to a shorter distance between adjacent Bi^{3+} ions, which is the main reason for concentration quenching phenomenon. [47] According to previous researches, the luminescence intensity (I) and doping concentration (x) can be expressed in the following Eq. (4):[48].

$$I \sim v = x\frac{\varphi_D}{\varphi_{D0}} \quad (4)$$

In turn, the PLQY is the ratio of the integrals of the luminescence decay kinetics with and without acceptors:[49–51].

$$\frac{\varphi_D}{\varphi_{D0}} = \frac{\int_0^\infty I_D(t)dt}{\int_0^\infty I_{D0}(t)dt} = \frac{\int_0^\infty e^{-t/\tau_D}N(t)dt}{\int_0^\infty e^{-t/\tau_D}dt} = \frac{1}{\tau_D}\int_0^\infty e^{-t/\tau_D}N(t)dt = \frac{\tau_{DA}}{\tau_D} \quad (5)$$

Here τ_D is the proper time of the donor's radiative decay, and $N(t)$ is the kinetics of concentration quenching, which is the object of close attention of the theory. With an increase in the donor concentration, the rate of migration of excitations through the system of impurity donor centers increases, which ensures efficient delivery of excitations to acceptors. This system contains channels of cross-relaxation of excitation, then the role of energy acceptors can be played by the unexcited donors themselves, thus, Bi^{3+} ions in LSS are self-quenching model. In addition, we detected the luminescent kinetics properties of LSS phosphors doping different Bi^{3+} concentration, and the decay curves (λ_{ex} = 375 nm, λ_{em} = 530 nm) of LSS: xBi^{3+} (x = 0.3%–3.0%) in Fig. 4**e**. The fitting lifetime values were calculated via the double-exponential model due to the existence of two Bi^{3+} luminescent centers (Fig. 4**f**). With increasing Bi^{3+} concentration, lifetime value first increases from 615 ns of x = 0.3% to 633 ns of x = 1.0%, then the decreases to 592 ns of x = 3.0%. This result is in

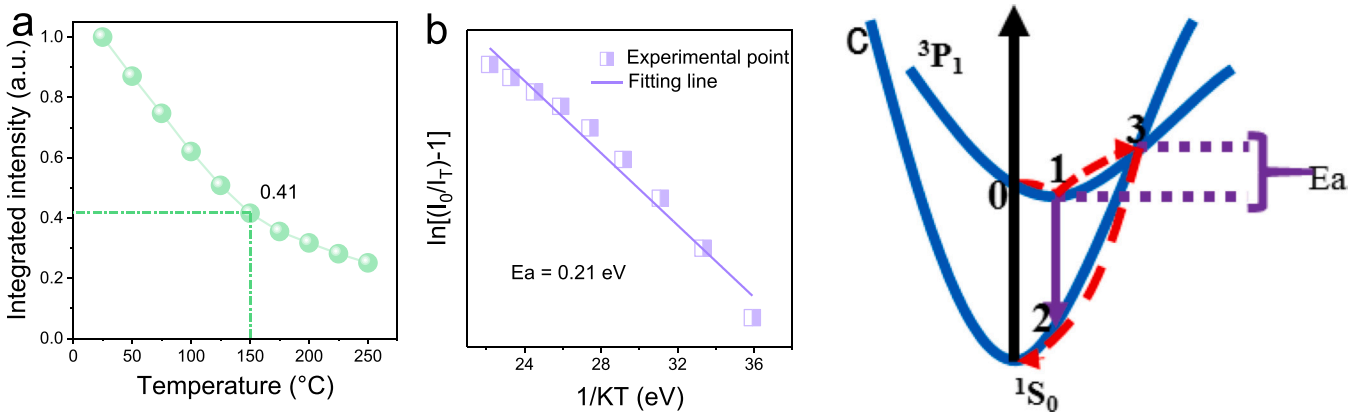

Fig. 5. (a) The integrated temperature-dependent PL spectra of LSS: 1.0%Bi^{3+} phosphor under 340 nm excitation in the temperature range of 25 – 250 °C with a temperature interval of 25 °C. (b) Arrhenius fitting of the integrated intensity in LSS: 1.0%Bi^{3+} phosphor. (c)The schematic configuration coordinate diagram of Bi^{3+}.

good accordance with the PLQY and PL intensity variation and give a further evidence for the quenching mechanism.

The thermal stability of phosphors is an essential parameter to assess their practical applications in pc-WLED devices. Hence, the temperature-dependent PL intensity of LSS: 1.0%Bi^{3+} phosphor was collected under 340 nm excitation in the temperature range of 25–250 °C with a temperature interval of 25 °C. From Fig. 5**a**, the temperature-dependent integrated intensity of LSS:1.0%Bi^{3+} phosphor shows a continuous decrease with increasing temperature. At 150 °C, the integrated intensity only remains 0.41 of that at 25 °C, which implies that serious thermal quenching phenomenon occurs during rising temperature. To better understand the process of thermal quenching, activation energy (E_a) is calculated by Arrhenius equation: [52,53].

$$I_T = \frac{I_0}{1 + A\exp(-E_a/kT)} \tag{6}$$

where I_T and I_0 represent integrated PL intensity at testing temperature and initial room temperature, respectively. A is a constant for a certain host, and k stands for Boltzmann constant (8.629×10^{-5} eV). According to Eq. (6), the calculated E_a value is 0.21 eV for LSS: 1.0%Bi^{3+} phosphor. The smaller E_a value would imply the weak thermal stability of LSS: xBi^{3+} (x = 0.3%–3.0%) phosphors. In order to clearly understand the thermal quenching phenomenon, Fig. 5**c** shows the configuration coordinate diagram of Bi^{3+} in LSS host. At room temperature, the electrons jump to $^1P_1$ and $^3P_1$ excited states upon the excitation of n-UV/UV or blue chips, respectively. Thereafter, the electrons return to $^1S_0$ ground state through the path of 0→1→2 with green emission. However, as temperature increases, electrons easily jump to the crossover point between $^3P_1$ and $^1S_0$, which leads to nonradiative transition to the ground state through the path of 0→1→3→2. Namely, the nonradiative transition is responsible for thermal quenching phenomenon. In theory, the higher E_a value would provide a harder environment for electrons to jump to the crossover point, which could reduce the possibility that electrons return to ground state by nonradiative path [24,54]. Therefore, the smaller E_a value would be responsible for the weak thermal stability of LSS: Bi^{3+} phosphors.

3.2. The energy transfer strategy in LSS: 1.0%Bi^{3+}, yEu^{3+} (y = 0.5–5.0%) phosphors

Energy transfer strategy is a reliable method to improve the luminescence properties of phosphors. Therefore, the energy transfer strategy from Bi^{3+} to Eu^{3+} was designed in LSS host to monitor the photoluminescence color by fixing Bi^{3+} concentration and varying Eu^{3+} concentration. The XRD patterns of LSS: 1.0%Bi^{3+}, yEu^{3+} (y = 0.5%, 1.0%, 2.0%, 3.0%, 5.0%) phosphors and standard LSS data are shown in Fig. 6**a**, which indicates the phase purity of theses samples due to no extra phase. In other words, the structure of LSS host has no significant change after co-doping Bi^{3+} and Eu^{3+} ions. To attest the successful introduction of Bi^{3+} and Eu^{3+} into LSS host, the XPS spectra of LSS: 1.0%Bi^{3+}, 5.0%Eu^{3+} phosphors about Bi^{3+} and Eu^{3+} elements were also measured. In Fig. 6**b**, the peaks located at

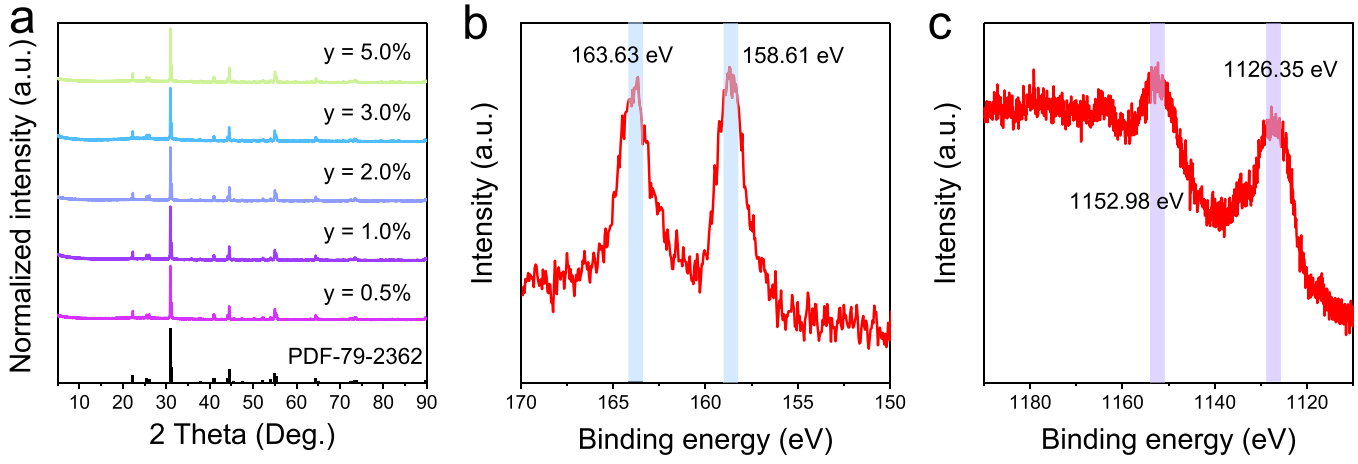

Fig. 6. (a) The XRD patterns of LSS: 1.0%Bi^{3+}, yEu^{3+} (y = 0.5%, 1.0%, 2.0%, 3.0%, 5.0%) phosphors and the standard LSS data. The XPS spectra of (b) Bi and (c) Eu elements in LSS: 1.0% Bi^{3+}, 5.0%Eu^{3+} phosphor.

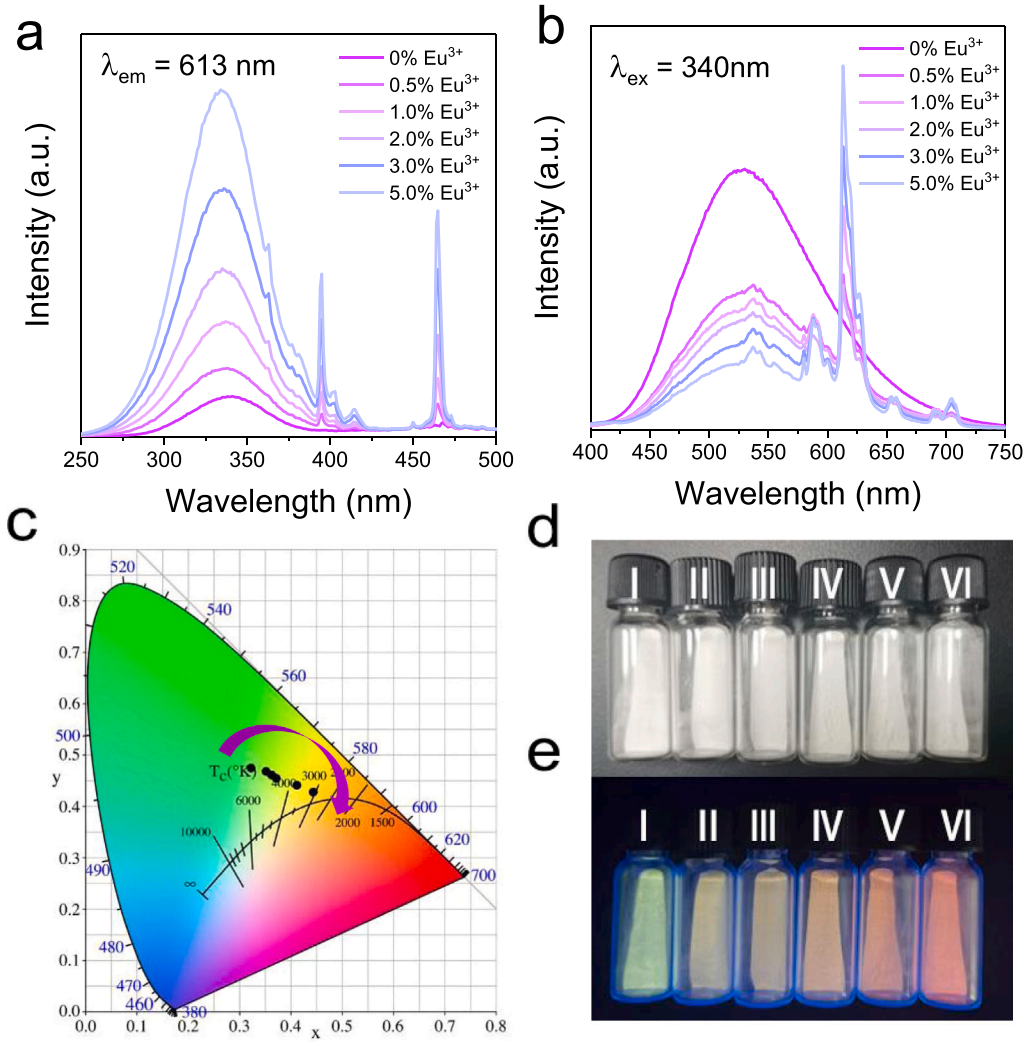

Fig. 7. (a) PLE (λ_{em} = 613 nm), (b) PL (λ_{ex} = 340 nm) spectra, and (c) corresponding chromaticity coordinates diagram and of LSS: 1.0%Bi^{3+}, yEu^{3+} (y = 0, 0.5%, 1.0%, 2.0%, 3.0%, 5.0%) phosphors. The luminescence photographs of LSS: 1.0%Bi^{3+}, yEu^{3+} (y = 0, 0.5%, 1.0%, 2.0%, 3.0%, 5.0%) phosphors under (d) natural light and (e) 365 nm n-UV light, in which I-VI corresponds to Eu^{3+} concentration of 0%, 0.5%, 1.0%, 2.0%, 3.0%, 5.0%, respectively.

163.63 eV and 158.61 eV represent the existence of trivalent Bi elements. Similarly, peaks situated in 1152.98 eV and 1126.35 eV correspond to trivalent Eu element in Fig. 6**c**. [55] As a result, Bi^{3+} and Eu^{3+} ions were successfully doped into LSS host at the same time.

The PLE (λ_{em} = 613 nm) and PL (λ_{ex} = 340 nm) spectra of LSS: 1.0% Bi^{3+}, yEu^{3+} (y = 0, 0.5%, 1.0%, 2.0%, 3.0%, 5.0%) phosphors are shown in Figs. 7**a** and 7**b**. The PLE spectra (λ_{em} = 613 nm) of LSS: 1.0%Bi^{3+}, yEu^{3+} (y = 0. 0.5%, 1.0%, 2.0%, 3.0%, 5.0%) phosphors show excitation band in the range of 250–500 nm peaking at ~340, ~394, and ~464 nm. The excitation peak around 340 nm is ascribed to $^1S_0 \rightarrow {}^1P_1/{}^3P_1$ transitions of Bi^{3+} with $O^{2-} \rightarrow Eu^{3+}$ charge transfer transition. The other excitation peaks (394, 464 nm) are attributed to $^7F_0 \rightarrow {}^5L_6$, and $^5D_2$ of Eu^{3+}, respectively [25,28]. Under 340 nm excitation, the PL spectra of LSS: 1.0%Bi^{3+}, yEu^{3+} (y = 0, 0.5%, 1.0%, 2.0%, 3.0%, 5.0%) show two types of strong emission peaks located at 530 nm and 613 nm, which correspond to $^3P_1 \rightarrow {}^1S_0$ transitions of Bi^{3+} ions and characteristic transition of Eu^{3+} ions, respectively. The strongest emission of Eu^{3+} ions is located at 613 nm, which is attributed to $^5D_0 \rightarrow {}^7F_2$ transition of Eu^{3+} ions. Besides, other emission peaks of Eu^{3+} are mainly located at ~588 nm ($^5D_0 \rightarrow {}^7F_1$), ~656 nm ($^5D_0 \rightarrow {}^7F_3$), and ~704 nm ($^5D_0 \rightarrow {}^7F_4$) [56,57]. On the basis of PL spectra of LSS: 1.0%Bi^{3+}, yEu^{3+} (y = 0, 0.5%, 1.0%, 2.0%, 3.0%, 5.0%) phosphors, the luminescence intensity of Bi^{3+} peaking at 530 nm shows a decreasing trend and emission of Eu^{3+} increases with the increase of Eu^{3+} concentration, which means that the energy transfer from Bi^{3+} to Eu^{3+} would happen. In Fig. 7**c**, the chromaticity coordinates diagram of LSS: 1.0%Bi^{3+}, yEu^{3+} (y = 0, 0.5%, 1.0%, 2.0%, 3.0%, 5.0%) phosphors shifts from (0.3223, 0.4747) to (0.4458, 0.4247) with increasing Eu^{3+} concentration, realizing the color tuning from green to orange. In order to clearly present the color changing, the photographs of these LSS: 1.0%Bi^{3+}, yEu^{3+} (y = 0, 0.5%, 1.0%, 2.0%, 3.0%, 5.0%) phosphors under natural light and 365 nm n-UV light are shown in Figs. 7**d** and 7**e**. Under natural light illuminating, the colors of these powers are white. Obviously, luminescent color varies from green light to orange light under 365 nm n-UV light with the increase of Eu^{3+} concentration, which should be originated from the appearance of energy transfer from Bi^{3+} ions to Eu^{3+} ions.

Besides, the photoluminescence decay curves of Bi^{3+} in LSS: 1.0% Bi^{3+}, yEu^{3+} (y = 0, 0.5%, 1.0%, 2.0%, 3.0%, 5.0%) phosphors also provide the convincing evidence for energy transfer process. Fig. 8**a** shows the photoluminescence decay curves (λ_{ex} = 375 nm, λ_{em} = 530 nm) of LSS: 1.0%Bi^{3+}, yEu^{3+} (y = 0, 0.5%, 1.0%, 2.0%, 3.0%, 5.0%) phosphors. For these samples, decay curves can be well fitted in double-exponential model defined as the following Eq. (7): [58].

$$I(t)/I_0 = A_1 \exp(-t/\tau_1) + A_2 \exp(-t/\tau_2) \quad (7)$$

where t means time, $I(t)$ is the corresponding luminescence intensity, A_1 and A_2 represent constants, τ_1 and τ_2 stand for rapid or

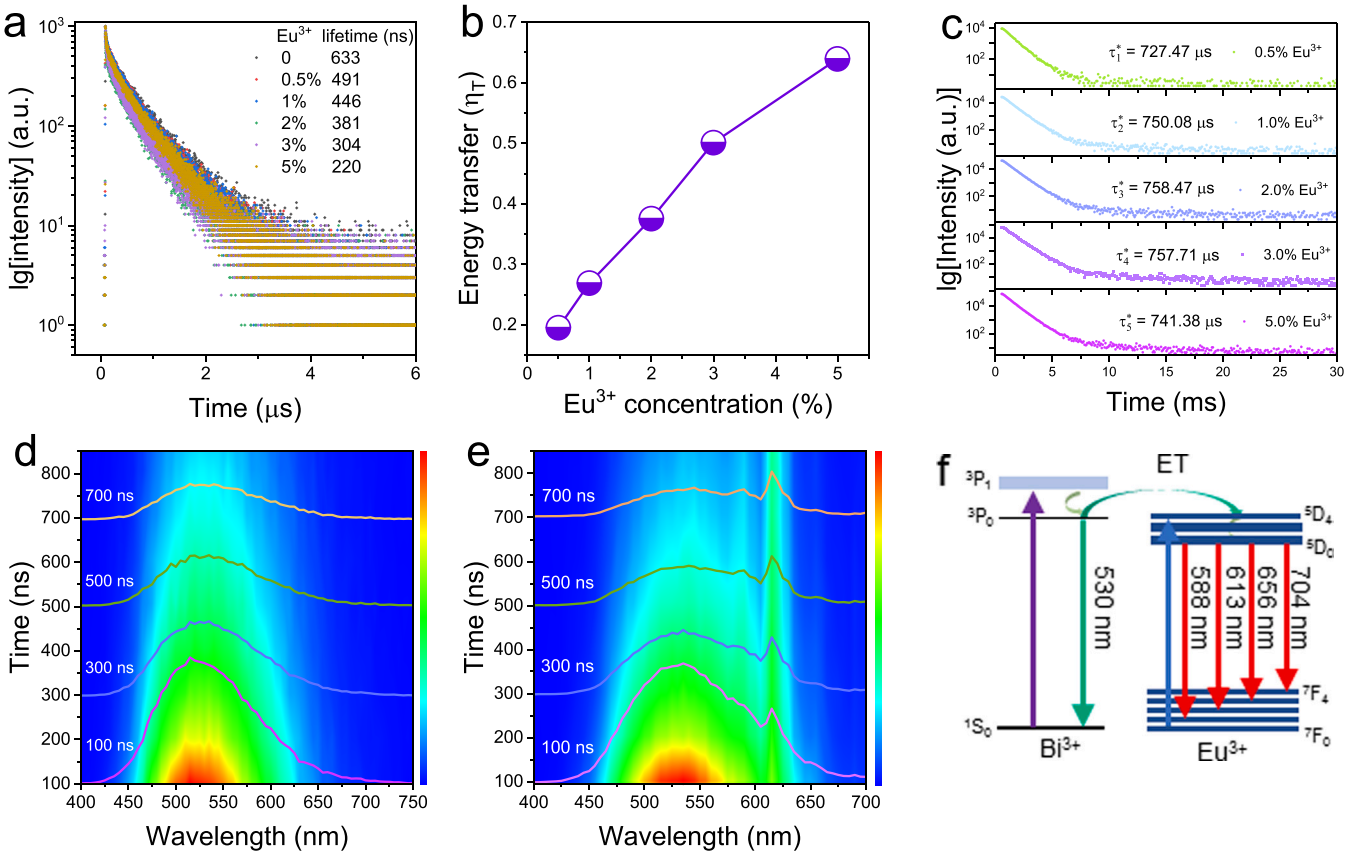

Fig. 8. (a) Photoluminescence decay curves of LSS: 1.0%Bi^{3+}, yEu^{3+} (y = 0, 0.5%, 1.0%, 2.0%, 3.0%, 5.0%) phosphors (λ_{ex} = 375 nm, λ_{em} = 530 nm). (b) The relationship between energy transfer efficiency η_T and Eu^{3+} concentration. (c) Photoluminescence decay curves of LSS: 1.0%Bi^{3+}, yEu^{3+} (y = 0.5%, 1.0%, 2.0%, 3.0%, 5.0%) phosphors (λ_{ex} = 340 nm, λ_{em} = 613 nm). Time-resolved emission spectra (TRES) and the representative PL curves collected at 100, 300, 500, 700 ns of the representative (d) LSS: 1.0%Bi^{3+} and (e) LSS: 1.0%Bi^{3+}, 5.0%Eu^{3+} phosphors. (f) The mechanism of energy transfer from Bi^{3+} to Eu^{3+}.

slow decay times, respectively. Based on Eq. (7), the value of average lifetime τ^* can be acquired by the expression below: [59].

$$\tau^* = \frac{1}{\tau_{DA}}\int_0^\infty t\left[\frac{I(t)}{I_0} = e^{-t/\tau_D}N(t)\right]dt = \frac{A_1\tau_1^2 + A_2\tau_2^2}{A_1\tau_1 + A_2\tau_2} \quad (8)$$

$$\tau_{DA} = \int_0^\infty \left[\frac{I(t)}{I_0} = e^{-t/\tau_D}N(t)\right]dt = A_1\tau_1 + A_2\tau_2 \quad (9)$$

where $N(t)$ is the kinetics of concentration quenching, which is the object of close attention of the theory. Consequently, the average lifetimes of Bi^{3+} in these phosphors were determined to be 633, 491, 446, 381, 304, and 220 ns, corresponding to Eu^{3+} concentration of y = 0, 0.5%, 1.0%, 2.0%, 3.0%, and 5.0%, respectively (Fig. 8**a**). The average lifetimes of Bi^{3+} show decreasing trend with increasing Eu^{3+} concentration in these samples. It strongly proves the existence of energy transfer from Bi^{3+} ions to Eu^{3+} ions in LSS: 1.0%Bi^{3+}, yEu^{3+} (y = 0, 0.5%, 1.0%, 2.0%, 3.0%, 5.0%) phosphors. In addition, energy transfer efficiency (η_T) from Bi^{3+} ions to Eu^{3+} ions can be calculated from the variation in lifetimes by Eq. (10): [60].

$$\eta_T = 1 - \frac{\tau_s^*}{\tau_0^*} \quad (10)$$

where τ_s^* and τ_0^* represent average lifetimes of Bi^{3+} ions in the presence and absence of Eu^{3+} ions, respectively. Energy transfer efficiency values are 0.224, 0.295, 0.398, 0.520, 0.652 for y = 0.5%, 1.0%, 2.0%, 3.0%, 5.0% in LSS: 1%Bi^{3+}, yEu^{3+} phosphors, respectively. These energy transfer efficiency values exhibit an increasing trend with rising Eu^{3+} concentration (Fig. 8**b**). On the other hand, the lifetimes of Eu^{3+} in LSS: 1.0%Bi^{3+}, yEu^{3+} (y = 0.5%, 1.0%, 2.0%, 3.0%, 5.0%) phosphors are also analyzed (Fig. 8**c**) (λ_{em} = 613 nm). According to Eq. (9), the average lifetimes of Eu^{3+} in LSS: 1.0%Bi^{3+}, yEu^{3+} (y = 0.5%, 1.0%, 2.0%, 3.0%, 5.0%) phosphors are 727.47, 750.08, 758.47, 757.71, 741.38 μs, respectively. With increasing Eu^{3+} concentration, the average lifetimes of Eu^{3+} show a fluctuant trend. In spite of this, the existence of energy transfer from Bi^{3+} to Eu^{3+} has been proved.

Additionally, time-resolved emission spectra (TRES) can analyze the dynamic process of energy transfer phenomenon. [61,62] Therefore, time-resolved emission spectra of the representative LSS: 1.0%Bi^{3+} and LSS: 1.0%Bi^{3+}, 5.0%Eu^{3+} phosphors were measured at 375 nm excitation and the representative emission curves collected at 100, 300, 500, and 700 ns are shown in Figs. 8**d** and 8**e**, respectively. Bi^{3+} luminescence (centered at 530 nm) is presented as broadband in range of 400–750 nm with much shorter decay time (nanosecond), and Eu^{3+} luminescence locates at 613 nm. However, comparing the decay time of Bi^{3+} in LSS: 1.0%Bi^{3+} phosphor and LSS: 1.0%Bi^{3+}, 5.0%Eu^{3+} phosphor, the Bi^{3+} in co-doping sample shows relative shorter decay time than that in LSS: 1.0%Bi^{3+} sample. In other words, energy transfer from Bi^{3+} to Eu^{3+} would be happened. Besides, it is necessary to explore relative intensity of Bi^{3+} and Eu^{3+} in co-doped sample to testify the existence of energy transfer. In Fig. 8**e**, these two types of peaks can be apparently observed at 100 ns. However, when the decay time exceeds 300 ns, the peak originated from Bi^{3+} becomes weak and even vanishes at 700 ns. Besides, the peak originated from Eu^{3+} shows an unconspicuously decreasing trend in comparison with the peak of Bi^{3+}. In general, with increasing decay time, all emission intensity of LSS: 1.0%Bi^{3+}, 5.0%Eu^{3+} phosphor becomes weak. Specially, according to the decay curves for representative 100, 300, 500 and 700 ns, the intensity of peak originated from Bi^{3+} shows a rapidly decreasing speed than the

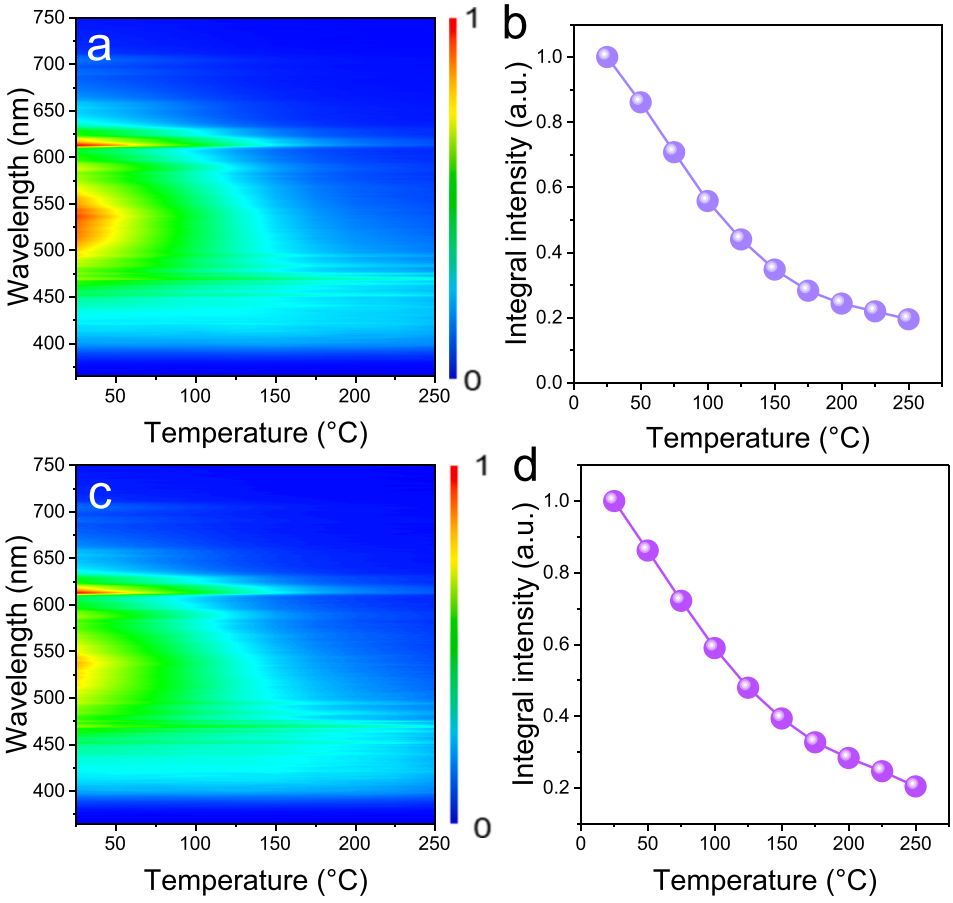

Fig. 9. (a) The PL spectra and (b) the normalized temperature-dependent PL spectra of LSS:1.0% Bi^{3+}, 0.5%Eu^{3+} under 340 nm excitation in the temperature range of 25–250 °C with a temperature interval of 25 °C. (c) The PL spectra and (d) the normalized temperature-dependent PL spectra of LSS:1.0% Bi^{3+}, 1.0%Eu^{3+} under 340 nm excitation in the temperature range of 25–250 °C with a temperature interval of 25 °C.

peaks attributed to Eu^{3+}. All these results prove that energy transfer from Bi^{3+} ions to Eu^{3+} ions exists in LSS: 1.0%Bi^{3+}, 5.0%Eu^{3+} phosphor.

The mechanism of energy transfer from Bi^{3+} to Eu^{3+} is summarize as Fig. 8f. When Bi^{3+} is excited by n-UV light, the electrons on the $^1S_0$ energy level (ground state) of Bi^{3+} could be excited to the $^3P_1$ energy level (higher excited state), and then relax to the lower excited state $^3P_0$ energy level. Due to the similar excited state energy level between Bi^{3+} and Eu^{3+}, the electrons have two ways to return to ground state. Firstly, part of electrons would return to $^1S_0$ energy level with characteristic Bi^{3+} emission (green light centered at 530 nm). Besides, other electrons would reach to the $^5D_4$ energy level (higher excited state of Eu^{3+}) via energy transfer progress (ET), and then relax to lower $^5D_0$ energy level. At the same time, the electrons of Eu^{3+} on the ground state are also excited to the higher excited state $^5D_4$ energy level and relax to the lower $^5D_0$ energy level. These electrons from two paths can return to the ^7F_j (j = 0–4) ground states and emit the characteristic red line emission of Eu^{3+}. The energy transfer progress can enhance emission intensity of Eu^{3+} and realize color adjustment from green to orange.[28].

As for thermal stability of LSS: 1.0%Bi^{3+}, yEu^{3+} (y = 0, 0.5%, 1.0%, 2.0%, 3.0%, 5.0%) samples, Figs. 9**a** and 9**c** show the temperature-dependent PL spectra of the representative LSS:1.0% Bi^{3+}, 0.5%Eu^{3+} and LSS: 1.0%Bi^{3+}, 1.0%Eu^{3+} phosphors under 340 nm excitation in the temperature range of 25 – 250 °C with a temperature interval of 25 °C. Obviously, the PL intensity of LSS: 1.0%Bi^{3+}, 0.5% Eu^{3+} and LSS: 1.0%Bi^{3+}, 1.0%Eu^{3+} phosphors gradually decreases with rising temperature. In Figs. 9**b** and 9**d**, the normalized temperature-dependent PL spectra of LSS: 1.0%Bi^{3+}, 0.5% Eu^{3+} and LSS: 1.0%Bi^{3+}, 1.0%Eu^{3+} phosphors also present sharply decreasing trend. For LSS: 1.0%Bi^{3+}, 0.5% Eu^{3+} phosphor, the integrated intensity at 75 °C keeps around 0.71 of that at room temperature. When the temperature attains 150 °C, the integrated intensity of LSS: 1.0%Bi^{3+}, 0.5% Eu^{3+} only performs 0.35 of that at room temperature. As for LSS: 1.0%Bi^{3+}, 1.0% Eu^{3+} phosphor, the integrated intensity shows 0.72 and 0.39 respectively under 75 °C and 150 °C of that at room temperature. All results indicate that the thermal stability of LSS: 1.0%Bi^{3+}, 0.5%Eu^{3+} and LSS: 1.0%Bi^{3+}, 1.0%Eu^{3+} phosphors is not good. The fast thermal quenching phenomenon is the results of Bi^{3+} and Eu^{3+} co-doping in the LSS host. According to previous section, the thermal quenching mechanism of Bi^{3+} has been explained. The coexistence of some Bi^{3+} and Eu^{3+} commonly entering LSS host would aggravate the lattice distortion degree, which corresponds to weaker structure rigidity. [63] Therefore, the co-doped phosphors show the fast thermal quenching phenomenon, and more efforts should be paid to improve the thermal stability of these LSS phosphors.

3.3. pc-WLED performance

In order to evaluate the practical application of LSS: Bi^{3+}, Eu^{3+} phosphors in pc-WLED device, two kinds of pc-WLED devices were fabricated by these LSS phosphors, some commercial phosphors and 370 nm InGaN chips. The electroluminescence (EL) spectra of pc-WLED devices are shown in Fig. 10. Fig. 10**a** shows the EL spectra of the pc-WLED (1) device fabricated by LSS: 1.0%Bi^{3+}, commercial blue $BaMgAl_{10}O_{17}$: Eu^{2+} phosphor, commercial $CaAlSiN_3$ red phosphor with 370 nm chip, which shows high color rendering index (CRI) (96.0) and low corrected color temperature (CCT) value (4306 K). Due to much stronger Eu^{3+} emission than Bi^{3+} in LSS: 1.0%Bi^{3+}, 5.0%

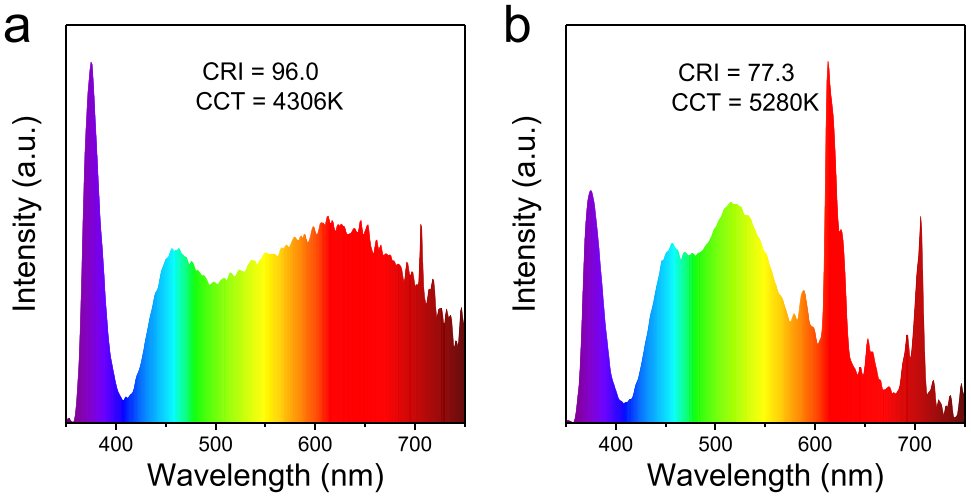

Fig. 10. (a) Electroluminescence (EL) spectra of pc-WLED (1) fabricated by LSS:1.0%Bi^{3+} phosphor, $BaMgAl_{10}O_{19}$: Eu^{2+} phosphor and commercial $CaAlSiN_3$ red phosphor with 370 nm InGaN chip. (b) Electroluminescence (EL) spectra of pc-WLED (2) fabricated by LSS: 1.0%Bi^{3+}, 5.0%Eu^{3+} phosphor, commercial blue $BaMgAl_{10}O_{19}$: Eu^{2+} phosphor, and commercial green $(Ba,Sr)_2SiO_4$: Eu^{2+} with 370 nm InGaN chips.

Eu^{3+} phosphor, the commercial green $(Ba,Sr)_2SiO_4$: Eu^{2+} phosphor were also added to pc-WLED (2) to acquire white emitting. Fig. 10**b** shows the EL spectrum of the pc-WLED (2) fabricated by LSS: 1.0% Bi^{3+}, 5.0%Eu^{3+} phosphor, commercial blue $BaMgAl_{10}O_{17}$: Eu^{2+} phosphor, and commercial green $(Ba,Sr)_2SiO_4$: Eu^{2+} phosphor with 370 nm chip. The values of CRI and CCT of pc-WLED (2) device are 77.3 and 5280 K, respectively. In conclusion, pc-WLED (1) realizes the warm white emitting (CRI = 96.0, CCT = 4306 K), while luminescent quality of pc-WLED (2) needs further optimize to obtain warm white emitting. Therefore, LSS: 1.0%Bi^{3+} phosphor can be the potential candidate for the practical application in pc-WLED devices.

4. Conclusion

Novel Bi^{3+}-doped and Bi^{3+}, Eu^{3+}-codoped LSS phosphors were successfully synthesized by a high-temperature solid-state method. LSS structure is composed of [La1/Sr1O_{12}], [La2/Sr2O_9], and [ScO_6] polyhedron. Bi^{3+} tends to occupy La site due to similar ionic radius. The band gap of LSS host is 2.08 eV, indicating that LSS is an appropriate host to accommodate activators. Under 340 nm excitation, LSS: Bi^{3+} phosphor shows wide-band green emission in range of 400–725 nm centering at 530 nm. According to the Gaussian fitting analysis, there are two fitting peaks in the emission peak of the representative LSS: 1.0%Bi^{3+} phosphor, which corresponds to the two types of La^{3+} sites for Bi^{3+} occupying. The concentration quenching mechanism of LSS: Bi^{3+} phosphor is dipole–dipole interaction. When temperature reaches 150 °C, the integral intensity remains only 0.41 of that at room temperature. So that more efforts should be made to improve the thermal stability of LSS: Bi^{3+} phosphors. On the other hand, by designing energy transfer strategy from Bi^{3+} ions to Eu^{3+} ions, the tunable emission color from green to orange is realized in LSS host. The average lifetimes of Bi^{3+} in LSS: 1.0%Bi^{3+}, yEu^{3+} (y = 0, 0.5%, 1.0%, 2.0%, 3.0%, 5.0%) present a decreasing trend with the increase of Eu^{3+} concentration. The energy transfer efficiency also increases with increasing Eu^{3+} concentration. The corresponding CIE chromaticity coordinates position shifts from (0.3223, 0.4747) to (0.4458, 0.4247). In TRES spectra of LSS: 1.0%Bi^{3+} and LSS: 1.0%Bi^{3+}, 5.0%Eu^{3+} phosphors, the emission intensity of Bi^{3+} in co-doping sample shows weaker intensity than that in LSS: 1.0%Bi^{3+} sample. Also, the peak of Eu^{3+} shows better emission intensity than the peak of Bi^{3+} with increasing decay time in LSS: 1.0%Bi^{3+}, 5.0%Eu^{3+} sample. All these results prove that the energy transfer happens in these LSS: 1.0%Bi^{3+}, yEu^{3+} (y = 0, 0.5%, 1.0%, 2.0%, 3.0%, 5.0%) phosphors. The pc-WLED (1) fabricated by LSS: 1.0%Bi^{3+} phosphor and commercial blue $BaMgAl_{10}O_{19}$: Eu^{2+} phosphor with 370 nm InGaN chip shows relatively high CRI (96.0) and low CCT (4306 K), demonstrating that LSS phosphors can be potential candidate for practical application of pc-WLED devices.

CRediT authorship contribution statement

All authors contribute themselves in this work. Guogang Li designed the system, Wei Yan and Yi Wei conducted the experiment, analyzed the data and wrote the manuscript, Maxim S. Molokeev completed the XRD refinement section. During the revision of this manuscript, the Dr. Song Wang give us a lot of useful suggestion and help us to measure and analyze the photoluminescence decay curves, PL spectra and write the cover letter responses. He gives a big contribution to this resubmission. Therefore, Dr. Wang is listed an co-corresponding author and all authors agreed with this change.

Declaration of Competing Interest

There are no conflicts to declare.

Acknowledgments

This work was supported by the National Natural Science Foundation of China (Grant Nos. 52072349).

References

[1] R. Gautier, X. Li, Z. Xia, F. Massuyeau, Two-step design of a single-doped white phosphor with high color rendering, J. Am. Chem. Soc. 139 (2017) 1436–1439, https://doi.org/10.1021/jacs.6b12597
[2] W.B. Im, N.N. Fellows, S.P. DenBaars, R. Seshadri, Y.-I. Kim, $LaSr_2AlO_5$, a versatile host compound for Ce^{3+}-based yellow phosphors: structural tuning of optical properties and use in solid-state white lighting, Chem. Mater. 21 (2009) 2957–2966, https://doi.org/10.1021/cm9006876
[3] S. Pimputkar, J.S. Speck, S.P. DenBaars, S. Nakamura, Prospects for LED lighting, Nat. Photon. 3 (2009) 180–182, https://doi.org/10.1038/nphoton.2009.32
[4] L. Wang, R.-J. Xie, T. Suehiro, T. Takeda, N. Hirosaki, Down-conversion nitride materials for solid state lighting: recent advances and perspectives, Chem. Rev. 118 (2018) 1951–2009, https://doi.org/10.1021/acs.chemrev.7b00284
[5] Z. Xia, R.-S. Liu, Tunable blue-green color emission and energy transfer of $Ca_2Al_3O_6F$:Ce^{3+},Tb^{3+} phosphors for near-UV white LEDs, J. Phys. Chem. C 116 (2012) 15604–15609, https://doi.org/10.1021/jp304722z
[6] V. Bachmann, C. Ronda, A. Meijerink, Temperature quenching of yellow Ce^{3+} luminescence in YAG:Ce, Chem. Mater. 21 (2009) 2077–2084, https://doi.org/10.1021/cm8030768

[7] M. Hermus, P.-C. Phan, A.C. Duke, J. Brgoch, Tunable optical properties and increased thermal quenching in the blue-emitting phosphor series: $Ba_2(Y_{1-x}Lu_x)_5B_5O_{17}:Ce^{3+}$ (x = 0–1), Chem. Mater. 29 (2017) 5267–5275, https://doi.org/10.1021/acs.chemmater.7b01416

[8] H. Zhu, C.C. Lin, W. Luo, S. Shu, Z. Liu, Y. Liu, et al., Highly efficient non-rare-earth red emitting phosphor for warm white light-emitting diodes, Nat. Commun. 5 (2014), https://doi.org/10.1038/ncomms5312

[9] K.A. Denault, J. Brgoch, M.W. Gaultois, A. Mikhailovsky, R. Petry, H. Winkler, et al., Consequences of optimal bond valence on structural rigidity and improved luminescence properties in $Sr_xBa_{2-x}SiO_4:Eu^{2+}$ orthosilicate phosphors, Chem. Mater. 26 (2014) 2275–2282, https://doi.org/10.1021/cm500116u

[10] J. Grigorjevaite, A. Katelnikovas, Luminescence and luminescence quenching of $K_2Bi(PO_4)(MoO_4):Eu^{3+}$ phosphors with efficiencies close to unity, ACS Appl. Mater. Interfaces 8 (2016) 31772–31782, https://doi.org/10.1021/acsami.6b11766

[11] M. Zhao, H. Liao, M.S. Molokeev, Y. Zhou, Q. Zhang, Q. Liu, et al., Emerging ultra-narrow-band cyan-emitting phosphor for white LEDs with enhanced color rendition, Light Sci. Appl. 8 (2019), https://doi.org/10.1038/s41377-019-0148-8

[12] X. Li, L. Zhou, J. Hong, S. He, X. Jing, M.D. Dramićanin, et al., Structural modulation induced intensity enhancement of full color spectra: a case of $Ba_3ZnTa_{2-x}Nb_xO_9:Eu^{3+}$ phosphors, J. Mater. Chem. C 8 (2020) 6715–6723, https://doi.org/10.1039/d0tc01201g

[13] M. Shang, S. Liang, N. Qu, H. Lian, J. Lin, Influence of anion/cation substitution ($Sr^{2+} \rightarrow Ba^{2+}$, $Al^{3+} \rightarrow Si^{4+}$, $N^{3-} \rightarrow O^{2-}$) on phase transformation and luminescence properties of $Ba_3Si_6O_{15}:Eu^{2+}$ phosphors, Chem. Mater. 29 (2017) 1813–1829, https://doi.org/10.1021/acs.chemmater.6b05493

[14] X. Wang, T. Seto, Z. Zhao, Y. Li, Q. Wu, H. Li, et al., Preparation of $Sr_{1-x}Ca_xYSi_4N_7:Eu^{2+}$ solid solutions and their luminescence properties, J. Mater. Chem. C 2 (2014) 4476–4481, https://doi.org/10.1039/c4tc00190g

[15] X. Zhang, Y.-T. Tsai, S.-M. Wu, Y.-C. Lin, J.-F. Lee, H.-S. Sheu, et al., Facile atmospheric pressure synthesis of high thermal stability and narrow-band red-emitting $SrLiAl_3N_4:Eu^{2+}$ phosphor for high color rendering index white light-emitting diodes, ACS Appl. Mater. Interfaces 8 (2016) 19612–19617, https://doi.org/10.1021/acsami.6b05485

[16] G. Xing, Z. Gao, M. Tao, Y. Wei, Y. Liu, P. Dang, et al., Novel orange-yellow-green color-tunable Bi^{3+}-doped $Ba_3Y_{4-w}Lu_wO_9$ ($0 \le w \le 4$) luminescent materials: site migration and photoluminescence control, Inorg. Chem. Front. 6 (2019) 3598–3603, https://doi.org/10.1039/c9qi01099h

[17] X. Huang, J. Liang, S. Rtimi, B. Devakumar, Z. Zhang, Ultra-high color rendering warm-white light-emitting diodes based on an efficient green-emitting garnet phosphor for solid-state lighting, Chem. Eng. J. 405 (2021) 126950, https://doi.org/10.1016/j.cej.2020.126950

[18] P. Dang, S. Liang, G. Li, Y. Wei, Z. Cheng, H. Lian, et al., Controllable optical tuning and improvement in Li^+,Eu^{3+}-codoped $BaSc_2O_4:Bi^{3+}$ based on energy transfer and charge compensation, J. Mater. Chem. C. 6 (2018) 6449–6459, https://doi.org/10.1039/C8TC01463A

[19] J. Han, L. Li, M. Peng, B. Huang, F. Pan, F. Kang, et al., Toward Bi^{3+} Red Luminescence with No Visible Reabsorption through Manageable Energy Interaction and Crystal Defect Modulation in Single Bi^{3+}-Doped $ZnWO_4$ Crystal, Chem. Mater. 29 (2017) 8412–8424, https://doi.org/10.1021/acs.chemmater.7b02979

[20] A. Huang, Z. Yang, C. Yu, Z. Chai, J. Qiu, Z. Song, Tunable and white light emission of a single-phased $Ba_2Y(BO_3)_2Cl:Bi^{3+}$,Eu^{3+} phosphor by energy transfer for ultraviolet converted white LEDs, J. Phys. Chem. C 121 (2017) 5267–5276, https://doi.org/10.1021/acs.jpcc.7b00019

[21] H. Li, R. Pang, G. Liu, W. Sun, D. Li, L. Jiang, et al., Synthesis and luminescence properties of Bi^{3+}-activated K_2MgGeO_4: a promising high-brightness orange-emitting phosphor for WLEDs conversion, Inorg. Chem. 57 (2018) 12303–12311, https://doi.org/10.1021/acs.inorgchem.8b02025

[22] J. Han, F. Pan, M.S. Molokeev, J. Dai, M. Peng, W. Zhou, et al., Redefinition of crystal structure and Bi^{3+} yellow luminescence with strong near-ultraviolet excitation in $La_3BWO_9:Bi^{3+}$ phosphor for white light-emitting diodes, ACS Appl. Mater. Interfaces 10 (2018) 13660–13668, https://doi.org/10.1021/acsami.8b00808

[23] D. Liu, X. Yun, P. Dang, H. Lian, M. Shang, G. Li, et al., Yellow/orange-emitting $ABZn_2Ga_2O_7:Bi^{3+}$(A = Ca, Sr; B = Ba, Sr) phosphors: optical temperature sensing and white light-emitting diode applications, Chem. Mater. 32 (2020) 3065–3077, https://doi.org/10.1021/acs.chemmater.0c00054

[24] Y. Wang, J. Ding, Y. Wang, Preparation and photoluminescence properties with the site-selected excitations of Bi^{3+}-activated $Ba_3Sc_4O_9$ phosphors, J. Am. Ceram. Soc. 100 (2017) 2612–2620, https://doi.org/10.1111/jace.14789

[25] P. Dang, S. Liang, G. Li, H. Lian, M. Shang, J. Lin, Broad color tuning of Bi^{3+}/Eu^{3+}-doped $(Ba,Sr)_3Sc_4O_9$ solid solution compounds via crystal field modulation and energy transfer, J. Mater. Chem. C 6 (2018) 9990–9999, https://doi.org/10.1039/c8tc03334j

[26] N. Wang, W. Zhao, J. Chen, J. Wang, Y. Meng, S. Yi, et al., Photoluminescence properties and charge compensation investigations of novel orange-emitting Eu^{3+} doped $Na_4Ca_4(Si_6O_{18})$ phosphors, J. Mater. Sci. Mater. Electron 27 (2016) 6681–6689, https://doi.org/10.1007/s10854-016-4615-1

[27] Y. Zhang, X. Zhang, H. Zhang, L. Zheng, Y. Zeng, Y. Lin, et al., Tunable emission from green to red in the $GdSr_2AlO_5:Tb^{3+}$,Eu^{3+} phosphor via efficient energy transfer, RSC Adv. 8 (2018) 3530–3535, https://doi.org/10.1039/c7ra12260h

[28] H. Zhou, Y. Jin, M. Jiang, Q. Wang, X. Jiang, A single-phased tunable emission phosphor $MgY_2Si_3O_{10}$: Eu^{3+}, Bi^{3+} with efficient energy transfer for white LEDs, Dalton Trans. 44 (2015) 1102–1109, https://doi.org/10.1039/c4dt02114b

[29] G. Li, Y. Tian, Y. Zhao, J. Lin, Recent progress in luminescence tuning of Ce^{3+} and Eu^{2+}-activated phosphors for pc-WLEDs, Chem. Soc. Rev. 44 (2015) 8688–8713, https://doi.org/10.1039/c4cs00446a

[30] Z. Xia, Q. Liu, Progress in discovery and structural design of color conversion phosphors for LEDs, Prog. Mater. Sci. 84 (2016) 59–117, https://doi.org/10.1016/j.pmatsci.2016.09.007

[31] K. Li, H. Lian, M. Shang, J. Lin, A novel greenish yellow-orange red $Ba_3Y4O_9:Bi^{3+}$,Eu^{3+} phosphor with efficient energy transfer for UV-LEDs, Dalton Trans. 44 (2015) 20542–20550, https://doi.org/10.1039/c5dt03565a

[32] W. Song, X. Chen, L. Teng, Z. Zheng, J. Wen, F. Hu, et al., Energy transfer and color-tunable emission in $Ba_2Y_2Si_4O_{13}:Bi^{3+}$,$Eu^{3+}$ phosphors, J. Am. Ceram. Soc. (2018), https://doi.org/10.1111/jace.16048

[33] H. Wang, X. Chen, L. Teng, D. Xu, W. Chen, R. Wei, et al., Adjustable emission and energy transfer process in $BaGd_2O_4:Bi^{3+}$,Eu^{3+} phosphors, J. Lumin. 206 (2019) 185–191, https://doi.org/10.1016/j.jlumin.2018.10.050

[34] D. Liu, P. Dang, X. Yun, G. Li, H. Lian, J. Lin, Luminescence color tuning and energy transfer properties in $(Sr,Ba)_2LaGaO_5:Bi^{3+}$,Eu^{3+} solid solution phosphors: realization of single-phased white emission for WLEDs, J. Mater. Chem. C 7 (2019) 13536–13547, https://doi.org/10.1039/c9tc04938j

[35] Y. Wang, J. Ding, Y. Li, L. Yang, X. Ding, Y. Wang, A novel single-phase warm white emission phosphor $Sr_3YAl_2O_{7.5}:Bi^{3+}$,Eu^{3+} with energy transfer for UV white LEDs, RSC Adv. 6 (2016) 42618–42626, https://doi.org/10.1039/c6ra05445e

[36] X. Chen, Z. Zheng, L. Teng, R. Wei, F. Hu, H. Guo, Self-calibrated optical thermometer based on luminescence from $SrLu_2O_4:Bi^{3+}$,Eu^{3+} phosphors, RSC Adv. 8 (2018) 35422–35428, https://doi.org/10.1039/c8ra06358c

[37] M. Xia, S. Gu, C. Zhou, L. Liu, Y. Zhong, Y. Zhang, et al., Enhanced photoluminescence and energy transfer performance of $Y_3Al_4GaO_{12}:Mn^{4+}$,Dy^{3+} phosphors for plant growth LED lights, RSC Adv. 9 (2019) 9244–9252, https://doi.org/10.1039/c9ra00700h

[38] S. Tamboli, P.D. Bhoyar, S.J. Dhoble, Analysis of electron-vibrational interaction in the 5d states of Eu^{2+} ions in $A_3P_4O_{13}$ and $A_3(PO_4)_2$ (A=Sr, Ba) phosphors, J. Lumin. 184 (2017) 23–28, https://doi.org/10.1016/j.jlumin.2016.12.003

[39] B. Wang, Y. Liu, Z. Huang, M. Fang, Photoluminescence properties of a Ce^{3+} doped $Sr_3MgSi_2O_8$ phosphor with good thermal stability, RSC Adv. 8 (2018) 15587–15594, https://doi.org/10.1039/c8ra00526e

[40] X. Wang, Z. Zhao, Q. Wu, C. Wang, Q. Wang, L. Yanyan, et al., Structure, photoluminescence and abnormal thermal quenching behavior of Eu^{2+}-doped $Na_3Sc_2(PO_4)_3$: a novel blue-emitting phosphor for n-UV LEDs, J. Mater. Chem. C. 4 (2016) 8795–8801, https://doi.org/10.1039/c6tc01049k

[41] T.T. Deng, E.H. Song, J. Sun, L.Y. Wang, Y. Deng, S. Ye, et al., The design and preparation of the thermally stable, Mn^{4+} ion activated, narrow band, red emitting fluoride $Na_3GaF_6:Mn^{4+}$ for warm WLED applications, J. Mater. Chem. C. 5 (2017) 2910–2918, https://doi.org/10.1039/c7tc00011a

[42] Y. Liu, J. Silver, R.-J. Xie, J. Zhang, H. Xu, H. Shao, et al., An excellent cyan-emitting orthosilicate phosphor for NUV-pumped white LED application, J. Mater. Chem. C. 5 (2017) 12365–12377, https://doi.org/10.1039/c7tc04168c

[43] X. Wang, J. Wang, X. Li, H. Luo, M. Peng, Novel bismuth activated blue-emitting phosphor $Ba_2Y_5B_5O_{17}:Bi^{3+}$ with strong NUV excitation for WLEDs, J. Mater. Chem. C. 7 (2019) 11227–11233, https://doi.org/10.1039/c9tc03729b

[44] R. Cao, G. Quan, Z. Shi, Z. Luo, Q. Hu, S. Guo, A double perovskite $Ca_2MgWO_6:Bi^{3+}$ yellow-emitting phosphor: Synthesis and luminescence properties, J. Lumin. 181 (2017) 332–336, https://doi.org/10.1016/j.jlumin.2016.09.046

[45] Y. Ding, N. Guo, X. Lü, H. Zhou, L. Wang, R. Ouyang, et al., None-rare-earth activated $Ca_{14}Al_{10}Zn_6O_{35}:Bi^{3+}$,$Mn^{4+}$ phosphor involving dual luminescent centers for temperature sensing, J. Am. Ceram. Soc. 102 (2019) 7436–7447, https://doi.org/10.1111/jace.16660

[46] X. Wang, Y. Wang, Synthesis, structure, and photoluminescence properties of Ce^{3+}-Doped $Ca_2YZr_2Al_3O_{12}$: a novel garnet phosphor for white LEDs, J. Phys. Chem. C 119 (2015) 16208–16214, https://doi.org/10.1021/acs.jpcc.5b01552

[47] M. Jiao, N. Guo, W. Lü, Y. Jia, W. Lv, Q. Zhao, et al., Tunable blue-green-emitting $Ba_3LaNa(PO_4)_3F:Eu^{2+}$,$Tb^{3+}$ phosphor with energy transfer for near-UV white LEDs, Inorg. Chem. 52 (2013) 10340–10346, https://doi.org/10.1021/ic401033u

[48] S.G. Fedorenko, A.V. Popov, E.A. Vagapova, A.E. Baranchikov, Y.V. Orlovskii, Concentration self-quenching of luminescence in crystal matrices activated by Nd^{3+} ions: theory and experiment, J. Lumin. 198 (2018) 138–145, https://doi.org/10.1016/j.jlumin.2018.02.032

[49] A.V. Popov, S.G. Fedorenko, V.A. Krut'ko, L.D. Iskhakova, M.G. Komova, E.E. Timofeeva, et al., Impurity fluorescence self-quenching in Nd^{3+}: Gd_3BWO_9 crystalline powders: experiment and analysis, J. Alloy. Compd. 822 (2020) 153654, https://doi.org/10.1016/j.jallcom.2020.153654

[50] W. Xiao, X. Zhang, Z. Hao, G.-H. Pan, Y. Luo, L. Zhang, et al., Blue-emitting $K_2Al_2B_2O_7:Eu^{2+}$ phosphor with high thermal stability and high color purity for near-UV-pumped white light-emitting diodes, Inorg. Chem. 54 (2015) 3189–3195, https://doi.org/10.1021/ic502773t

[51] H.F.L. Ozawa, P.M. Jaffe, G. Ban, The effect of exciting wavelength on optimum activator concentration, J. Electrochem. Soc. 118 (1971) 482–486, https://doi.org/10.1149/1.2408087

[52] H. Ming, J. Zhang, L. Liu, J. Peng, F. Du, X. Ye, et al., A novel $Cs_2NbOF_5:Mn^{4+}$ oxyfluoride red phosphor for light-emitting diode devices, Dalton Trans. 47 (2018) 16048–16056, https://doi.org/10.1039/c8dt02817f

[53] B. Wang, H. Lin, F. Huang, J. Xu, H. Chen, Z. Lin, et al., Non-rare-earth $BaMgAl_{10-2x}O_{17}:xMn^{4+}$,$xMg^{2+}$: a narrow-band red phosphor for use as a high-power warm w-LED, Chem. Mater. 28 (2016) 3515–3524, https://doi.org/10.1021/acs.chemmater.6b01303

[54] K. Li, R.Van Deun, Site-Bi^{3+} and Eu^{3+} dual emissions in color-tunable $Ca_2Y_8(SiO_4)_6O_2:Bi^{3+}$, Eu^{3+} phosphors prepared via sol-gel synthesis for potentially ratiometric temperature sensing, J. Alloy. Compd. 787 (2019) 86–95, https://doi.org/10.1016/j.jallcom.2019.02.087

[55] J. Xue, Y. Guo, B.K. Moon, S.H. Park, J.H. Jeong, J.H. Kim, et al., Improvement of photoluminescence properties of Eu^{3+} doped $SrNb_2O_6$ phosphor by charge compensation, Opt. Mater. 66 (2017) 220–229, https://doi.org/10.1016/j.optmat.2017.02.002
[56] Q. Cheng, F. Ren, Q. Lin, H. Tong, X. Miao, High quantum efficiency red emitting α-phase $La_2W_2O_9:Eu^{3+}$ phosphor, J. Alloy. Compd. 772 (2019) 905–911, https://doi.org/10.1016/j.jallcom.2018.08.320
[57] X. Zhang, H.J. Seo, Photoluminescence and concentration quenching of $NaCa_4(BO_3)_3:Eu^{3+}$ phosphor, J. Alloy. Compd. 503 (2010) L14–L17, https://doi.org/10.1016/j.jallcom.2010.04.242
[58] F.M. Emen, R. Altinkaya, Luminescence and thermoluminescence properties of $Sr_3WO_6:Eu^{3+}$ phosphor, J. Lumin. 134 (2013) 618–621, https://doi.org/10.1016/j.jlumin.2012.07.020
[59] J. Fu, S. Zhang, T. Ma, Y. Jia, R. Pang, L. Jiang, et al., A convenient and efficient synthesis method to improve the emission intensity of rare earth ion doped phosphors: the synthesis and luminescent properties of novel $SrO:Ce^{3+}$ phosphor, RSC Adv. 5 (2015) 93951–93956, https://doi.org/10.1039/c5ra15089b
[60] H. Chen, Y. Wang, $Sr_2LiScB_4O_{10}:Ce^{3+}/Tb^{3+}$: A Green-Emitting Phosphor with High Energy Transfer Efficiency and Stability for LEDs and FEDs, Inorg. Chem. 58 (2019) 7440–7452, https://doi.org/10.1021/acs.inorgchem.9b00639
[61] D. Hou, C. Liu, X. Ding, X. Kuang, H. Liang, S. Sun, et al., A high efficiency blue phosphor $BaCa_2MgSi_2O_8:Eu^{2+}$ under VUV and UV excitation, J. Mater. Chem. C 1 (2013) 493–499, https://doi.org/10.1039/c2tc00129b
[62] Y. Wei, H. Yang, Z. Gao, Y. Liu, G. Xing, P. Dang, et al., Strategies for designing antithermal-quenching red phosphors, Adv. Sci. 7 (2020) 1903060, https://doi.org/10.1002/advs.201903060
[63] M. Zhao, Z. Xia, M.S. Molokeev, L. Ning, Q. Liu, Temperature and Eu^{2+}-doping induced phase selection in $NaAlSiO_4$ polymorphs and the controlled yellow/blue emission, Chem. Mater. 29 (2017) 6552–6559 http://doi.org.10.1021/acs.chemmater.7b02548.